Time-resolved investigation of low-density plasma channels produced by a kilohertz femtosecond laser in air

Jiansheng Liu,* Zuoliang Duan, Zhinan Zeng, Xinhua Xie, Yunpei Deng, Ruxin Li, and Zhizhan Xu
State Key Laboratory of High Field Laser Physics, Shanghai Institute of Optics and Fine Mechanics, Chinese Academy of Sciences, P. O. Box 800-211, Shanghai 201800, People's Republic of China

See Leang Chin
Département de Physique, de Génie Physique et d'Optique and Centre d'Optique, Photonique et Laser (COPL), Université Laval, Québec, Canada G1K 7P4

(Received 16 May 2005; published 26 August 2005)

By employing pump-probe back longitudinal diffractometry, the electron density and decay dynamics of a weak plasma channel created by a 1-KHz fs laser in air has been investigated. With ultrashort laser pulses of 50 fs and low energy of 0.6 mJ, we observe weak plasma channels with a length ~2 cm in air. An analytical reconstruction method of electron density has been analyzed, which is sensitive to the phase shift and channel size. The electron density in the weak plasma channel is extracted to be about 4×10^{16} cm^{-3}. The diameters of the plasma channel and the filament are about 50 and 150 μm, respectively, and the measurable electron density can be extended to less than 10^{15} cm^{-3}. Moreover, a different time-frequency technique called linearly chirped longitudinal diffractometry is proposed to time-resolved investigate ultrafast ionization dynamics of laser-irradiated gas, laser interaction with cluster beam, etc.

DOI: 10.1103/PhysRevE.72.026412 PACS number(s): 52.35.Mw, 52.50.Jm, 52.40.Db, 52.80.Tn

I. INTRODUCTION

Plasma channels and self-phase matching excited by self-guided ultrafast laser pulses owing to the balance between the kerr self-focusing and defocusing due to the multiphoton ionization and diffraction of the laser beam is of much current interest owing to applications which include initiating laser-guided discharges, possible real lighting control, femtosecond lidar, conical emission, and high-order harmonics generation (HHG) [1–5]. In 1996, Braun *et al.* [5] observed self-focusing into filaments in air with infrared laser pulses. This effect was confirmed and reported by many other groups in the following years. The average initial electron density for a multifilamentary structure was estimated by Schillinger *et al.* to be $n_e>10^{11}$ cm^{-3}, whereas La Fontaine *et al.* and Tzortakis *et al.* estimated a value $n_e>10^{16}$ cm^{-3} for a single filament [6–9] and it was measured to be about 2.7×10^{18} cm^{-3} in Ref. [10]. The production of low-density electrons will balance the self-focusing effect and leads to a limited beam diameter as well as limited peak intensity. This is known as intensity clamping [11–13]. At such low densities, owing to the attachment of electrons to O_2, the electron-ion recombination, and the ion-ion recombination, the electron density in the plasma channel will decrease to the much lower level of $n_e>10^{15}$ cm^{-3} within several hundreds of picoseconds to several nanoseconds after the end of the laser pulse. Such sparse electrons could not be easily and nicely measured by interferometric methods such as Michelson and Wollaston interferometry [6,10], and the electric cross-conductivity technique [14]. In Ref. [6] where a longitudinal Michelson spectral interferometry was employed, the electron density was measured to be $\sim2\times10^{15}$ cm^{-3} which was revised to be around 10^{16}–10^{17} cm^{-3} by calculating the effect of radial refraction of the probe beam on the phase integration path length because a long filament of 1.5 m there would deviate the probe beam. In this paper, a pump-probe longitudinal diffractometry by measuring a much shorter plasma channel has been employed to investigate the temporal evolution of the electron density in the weak plasma channel created by a 1-KHz fs laser in air. The electron density in the weak plasma channel is extracted to be about 4×10^{16} cm^{-3}, and the diameters of the plasma channel and the filament are about 50 and 150 μm, respectively. The reconstruction method of electron density from diffraction patterns has been analyzed, and an analytical method is given which is sensitive to the phase shift and plasma channel size and therefore has a high precision and sensitivity. And the measurable electron density can be extended to less than 10^{15} cm^{-3}. Moreover, a different time-frequency technique called linearly chirped longitudinal diffractometry is first proposed to time-resolved investigate ultrafast ionization dynamics of laser-irradiated gas, laser interaction with cluster beam, etc. This method can be achieved by a single shot and is helpful for us to get insight into the physics of laser-matter interactions.

II. EXPERIMENTAL SETUP

In our experiments, the laser system is a 1-KHz Ti:sapphire fs laser system that can provide up to 0.6 mJ energy in 50-fs pulses and at a central wavelength of 800 nm. At the output of the laser, the beam profile is nearly Gaussian with a beam waist of $w_0=7$ mm. The laser beam was focused in air with a thin lens of focal length $f=40$ cm and formed a plasma channel. The electron density in the channel is estimated to be lower than 10^{17} cm^{-3} since the formed plasma channel is very weak and only can be discerned in a dark background. At such low-density level it is hard to identify

*Electronic address: michaeljs_liu@mail.siom.ac.cn

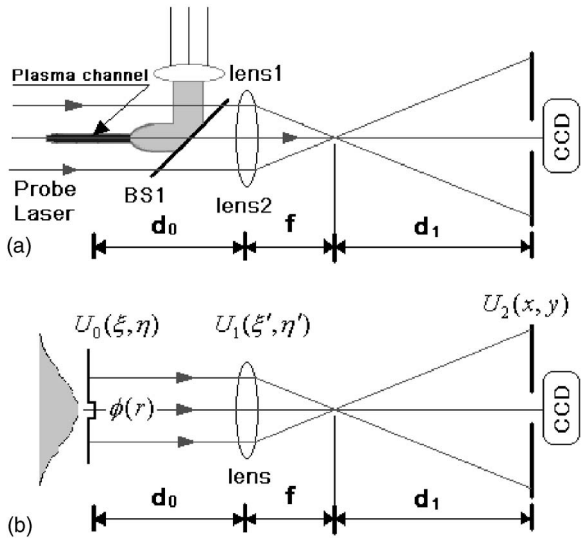

FIG. 1. (a) Experimental scheme for the time-resolved longitudinal diffraction interferometry. The laser beam (0.3 mJ, 50 fs, 800 nm) was focused in air with a thin lens of focal length $f=40$ cm and formed a plasma channel. The beam splitter BS1 has a reflectivity of 90% and transmissivity of 10%. The diffraction fringe pattern of the probe beam is recorded by a CCD camera at various delay times. (b) Schematic diagram for the propagation of a light field through a thin lens.

the electron density and the channel size by using Michelson or Wollaston interferometry. In order to have an insight into the temporal evolution of the electron density in the weak plasma channel, a pump-probe back longitudinal diffractometry has been developed to measure the electron density of less than 10^{16} cm^{-3}, which is sensitive to the phase and channel size, and the measurable electron density can be extended to less than 10^{15} cm^{-3}.

The experimental setup is shown in Fig. 1(a), and the schematic diagram for the propagation of a light field through a thin lens is shown in Fig. 1(b). The laser pulse from the 1-KHz laser system with energy of 0.6 mJ and pulse duration of 50 fs is divided by a beam splitter which has a reflectivity of 90% and transmissivity of 10%. The high-energy laser pulse was focused by a thin lens [lens 1 in Fig. 1(a)] of focal length $f=40$ cm and formed a plasma channel in air. The other low-energy pulse was used as a probe beam which anticopropagates against the direction of the formed weak plasma channel. The probe laser pulse after transmitting through the channel was diffracted by a lens onto a charge-coupled device (CCD) camera by which the diffraction pattern was recorded. The beam splitter in Fig. 1(a) which reflects most of the pump laser and transmits a small part of the probe beam has a reflectivity of 90% and transmissivity of 10%. From this diffraction pattern the phase shift experienced by the probe laser can be reconstructed, and thus the electron density and channel size can be obtained. Shown in Fig. 2 is the recorded diffraction pattern which is the subtraction of intensity distribution with a plasma channel by that without a channel, the delay time between the pump and probe laser pulse is zero.

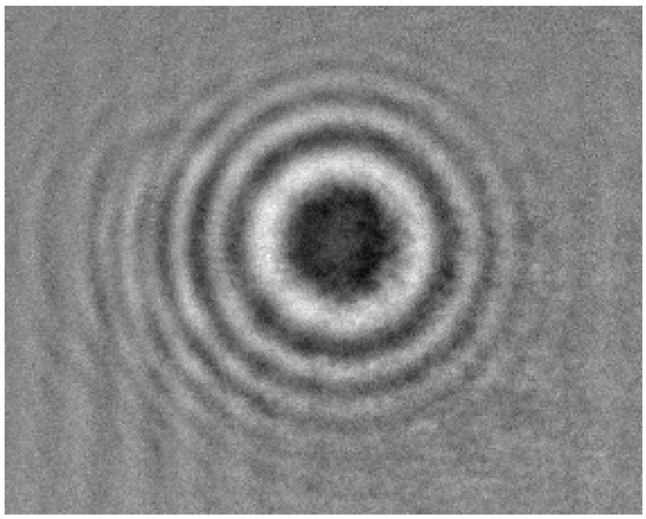

FIG. 2. The recorded diffraction fringe at delay time=0 ps.

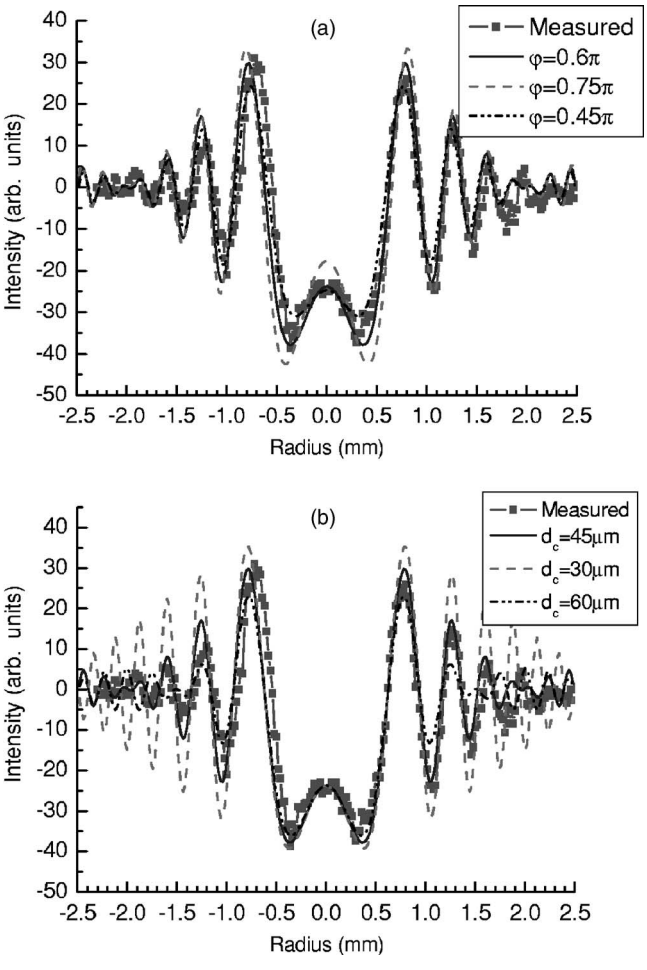

FIG. 3. (a) Measured diffraction fringe along the radial direction at delay time=0 ps compared with the fit lines at various phase shifts when the plasma channel size is set as 50 μm. (b) Compared with the fit lines at various channel sizes when the phase shift is set at $\sim 0.6\pi$.

III. ANALYSIS

As shown in Figs. 1(a) and 1(b), the light field of the probe laser pulse after transmitting through the plasma channel propagates through a thin lens; the plasma filament which has a small size with a diameter of about 50 μm plays the role of a local phase shifter for the probe laser pulse. At the distance d_1 from the lens' focus, a CCD camera is placed where the light field is expressed by the Fresnel diffraction integral [15],

$$U_2(x,y) \propto U(x,y) = \iiint\!\!\int U_0(\xi,\eta)\exp[-j\beta(\xi'^2+\eta^2)] \times\exp\{ja_0[(\xi'-\xi)^2+(\eta'-\eta)^2]\} \times\exp\{ja_1[(x-\xi')^2+(y-\eta')^2]\}d\xi d\eta d\xi' d\eta', \quad (1)$$

where $a_0=\pi/\lambda d_0$, $a_1=\pi/\lambda d_1$, $\beta=\pi/\lambda f$. d_0 is the length between the lens and the plasma channel, d_1 is the length between the lens and the CCD camera, and f is the focal length. $(\xi,\eta),(\xi',\eta')$, and (x,y) correspond to the coordinates in object, lens, and recording planes, respectively, which is shown in Fig. 1(b). After simplification,

$$U(x,y) = \exp[jA_0(x^2+y^2)] \times \iint U_0(\xi,\eta)\exp[jA_1(\xi^2+\eta^2)] \times\exp[-jA_2(x\xi+y\eta)]d\xi d\eta, \quad (2)$$

where $A_0=(\pi/\lambda d_1)[1-1/(1+d_1/d_0-d_1/f)]$, $A_1=(\pi/\lambda d_0)[1-1/(1+d_0/d_1-d_0/f)]$, $A_2=(2\pi/\lambda)[d_1+d_0-d_0d_1/f)$, and the probe electromagnetic field has a radial symmetry and can be written as $U_0(r)=\exp(-ar^2)\times\exp[-j\phi(r)]$, where the phase shift $\phi(r)$ caused by the plasma filament is assumed to be

$$\phi(r) = \begin{cases} \phi_0 & r \leqslant r_c \\ 0 & r > r_c \end{cases}. \quad (3)$$

r_c is the radius of the plasma filament, the accumulated phase $\phi(r)$ is related to the plasma density n_e by the relation $\phi_0=(2\pi/\lambda)(n_e/2n_c)l_{channel}$, where n_c is the plasma critical density and $l_{channel}$ is the length of the plasma filament. Owing to the small size of the filament compared to the waist of the probe laser beam, the integral in Eq. (2) can be divided into two parts:

$$U_{yes}(x,y) = \exp[jA_0(x^2+y^2)]\int\int_0^{r_c} + \int\int_{r_c}^{\infty} U_0(\xi,\eta)\exp[jA_1(\xi^2+\eta^2)]\exp[-jA_2(x\xi+y\eta)]d\xi d\eta = E_0e^{-j\phi_0}+E_1, \quad (4)$$

$$U_{no}(x,y) = \exp[jA_0(x^2+y^2)]\int\int_0^{r_c} + \int\int_{r_c}^{\infty} U_0(\xi,\eta)\exp[jA_1(\xi^2+\eta^2)]\exp[-jA_2(x\xi+y\eta)]d\xi d\eta = E_0+E_1. \quad (5)$$

The subscripts *yes* and *no* correspond to the diffracted light field with and without the effect of a plasma channel, respectively. E_0 is the Fraunhofer diffraction integral of a small circular hole because the quadratic phase term in the integral is very small and can be neglected. E_1 is the Fresnel diffraction integral of the probe beam with the channel area excluded and has the following Gaussian form:

$$E_1(r) \approx U_{no}(x,y) = C_0\exp(jA_0r^2)\exp(-b_0r^2-jb_1r^2+j\pi/2). \quad (6)$$

With some operations, the recorded diffraction pattern can be expressed as

$$\begin{aligned} I_d(r) &= I_{yes}(r) - I_{no}(r) \\ &= E_0e^{-j\phi_0}E_1^* - E_0E_1^* + \text{c.c.} \\ &= -\operatorname{sgn}(A_1)C\pi r_c^2\frac{1}{\sqrt{a^2+A_1^2}} \times\exp(-b_0r^2)\frac{J_1(A_2r_cr)}{A_2r_cr} \times\cos(b_1r^2-\phi_0/2)\sin(\phi_0/2), \end{aligned} \quad (7)$$

where $b_0=A_2^2a/4(a^2+A_1^2)$, $b_1=A_2^2A_1/4(a^2+A_1^2)$, and $\operatorname{sgn}(A_1)$ is the sign of A_1. Therefore the recorded diffraction pattern is the product of a Gaussian function, a Bessel function and an oscillating cosine function, which can explain the observed circle fringes shown in Fig. 2. The Bessel function in the above equation is the Fraunhofer diffraction of a circle hole, which is determined by the channel size. The size of the plasma channel has the effect on the relative amplitude of the different rings of the diffraction patterns while the phase shift has the effect on the brightness on the diffraction pattern. Therefore the size of the plasma channel and the phase shift can be determined at the same time by the diffraction pattern. From this equation, we can reconstruct the phase shift the probe beam experienced, and the size of the filament. In Fig. 3, we fit the recorded fringe pattern at delay time=0 by the above equation (6) with various phase shifts and channel sizes. [We note that the fitting result would be the same by numerically integrating Eq. (2) but the physical interpretation would be more cumbersome.] It is found that the recorded fringe profile along the radial direction can uniquely determine the phase shift and channel size. Moreover, it is not necessary for the calibration of the recorded intensity. From the comparison we found that only when the plasma channel size is set as $\sim$50 μm and the phase shift is set as

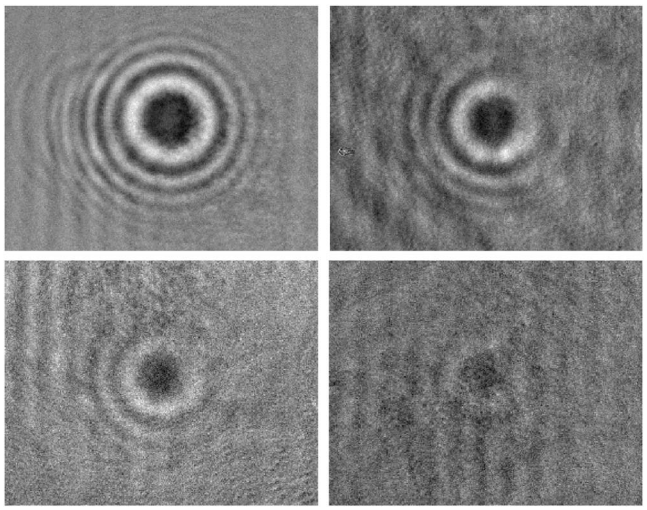

FIG. 4. The recorded fringe patterns at various delay time: 0, 100, 430, and 830 ps, respectively.

$\sim 0.6\pi$ at the same time, the fit will be closest to the measured diffraction pattern. Since the electrons in the plasma channel are produced by multiphoton ionization, the size of the filament can be calculated as about 150 μm if the profile of laser intensity in the filament is assumed as Gaussian and eight to ten photons are necessary to ionize O_2 molecules (ionization potential=12.1 eV) and N_2 molecules (ionization potential=15.6 eV). The measured size of the filament here is close to the result given as 150–170 μm in Ref. [16] where a windowless helium cell was used to measure directly the transverse profile of the filament. From the temporal measurement by adjusting the pump-probe delay, the length of the plasma channel in our experiment is calculated to be about $\sim$1.8 cm. The length is defined by the distance from the very weak appearance of the diffraction fringes through the maximum brightness and back to the weak fringes. Therefore the calculated electron density at delay time=0 is $\sim 4\times 10^{16}$ cm^{-3}. The recorded fringe patterns at various delay time=0, 100, 430 and 830 ps, respectively, are shown in Fig. 4, and the temporal evolution of

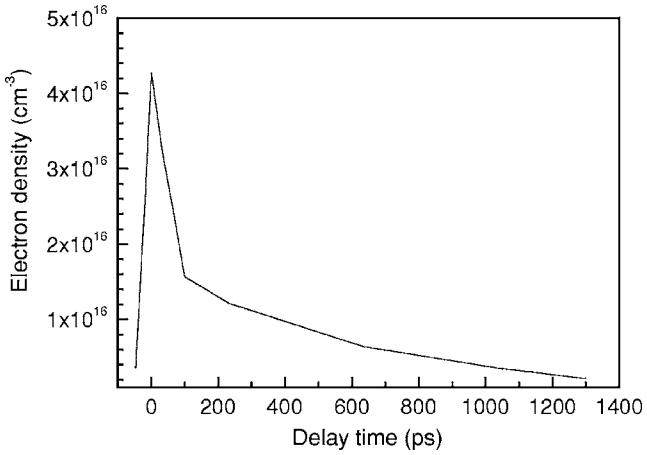

FIG. 5. Calculated temporal evolution of electron density in the plasma channel.

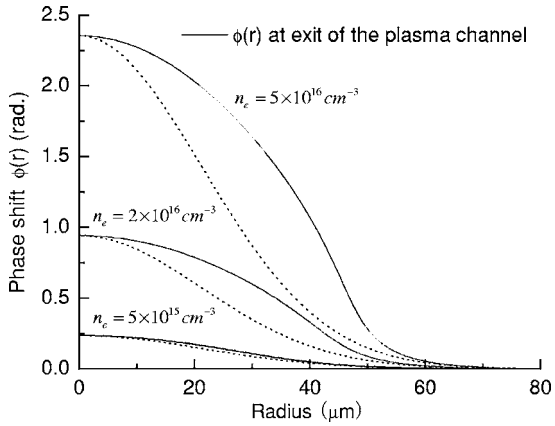

FIG. 6. The calculated phase shift experienced by the probe beam at the exit of the plasma channel when the electron densities are assumed as Gaussian and set at 5×10^{15}, 2×10^{16}, and 5×10^{16}cm^{-3}, respectively. Solid line: the phase shift $\phi(r)=\int_0^{l_{channel}}(2\pi/\lambda)[n_e(r)/2n_c]ds$ is calculated by solving the ray-tracing equation. Dashed line: the phase shift is calculated by a direct integration $\phi_0=(2\pi/\lambda)[n_e/2n_c]l_{channel}$.

electron density in the plasma channel is shown in Fig. 5. The calculations of electron density and channel size for various delay time have shown that the expansion of the plasma channel can be neglected in less than 1 ns after the production of the filament.

In our analysis, the electron density along the filament and radial direction is assumed to be constant, therefore the calculated electron density is an effective value as measured in Refs. [6,7,12]. Since the laser intensity in the filament has a radial gradient, the electron density in the plasma channel caused by multiphoton ionization would have also a radial gradient. If the electron density is too high and the probe beam passes through a too long plasma channel, the probe beam will be very likely to deviate from its path because of refraction on the steep radial gradients of electron density present in the filament, which will make exact measurement of electron density difficult. We use ray tracing to estimate the effect of radial refraction caused by the plasma channel on the measured phase shift experienced by the probe beam. The electron density in the plasma channel is assumed as a radial Gaussian profile and uniform in the direction of propagation. $n_e(r)=n_e(0)\exp(-0.69r^2/R^2)$, where $n_e(0)$ is the maximum electron density on axis, R is the radius (full width at half maximum) of the plasma channel. The refractive index $n(r)$ in the plasma channel can be expressed as

$$n(r) \approx 1 - \frac{n_e(0)}{2n_c}\exp(-0.69r^2/R^2) \tag{8}$$

and the propagation of the rays along the plasma channel can be described by the following equation of ray tracing [17]:

$$\frac{d}{ds}\left(n(r)\frac{dr}{ds}\right) = \nabla n(r), \tag{9}$$

where ds is the distance the rays propagate. By solving the above equation we can estimate the effect of radial refraction caused by the plasma channel on the measured phase shift

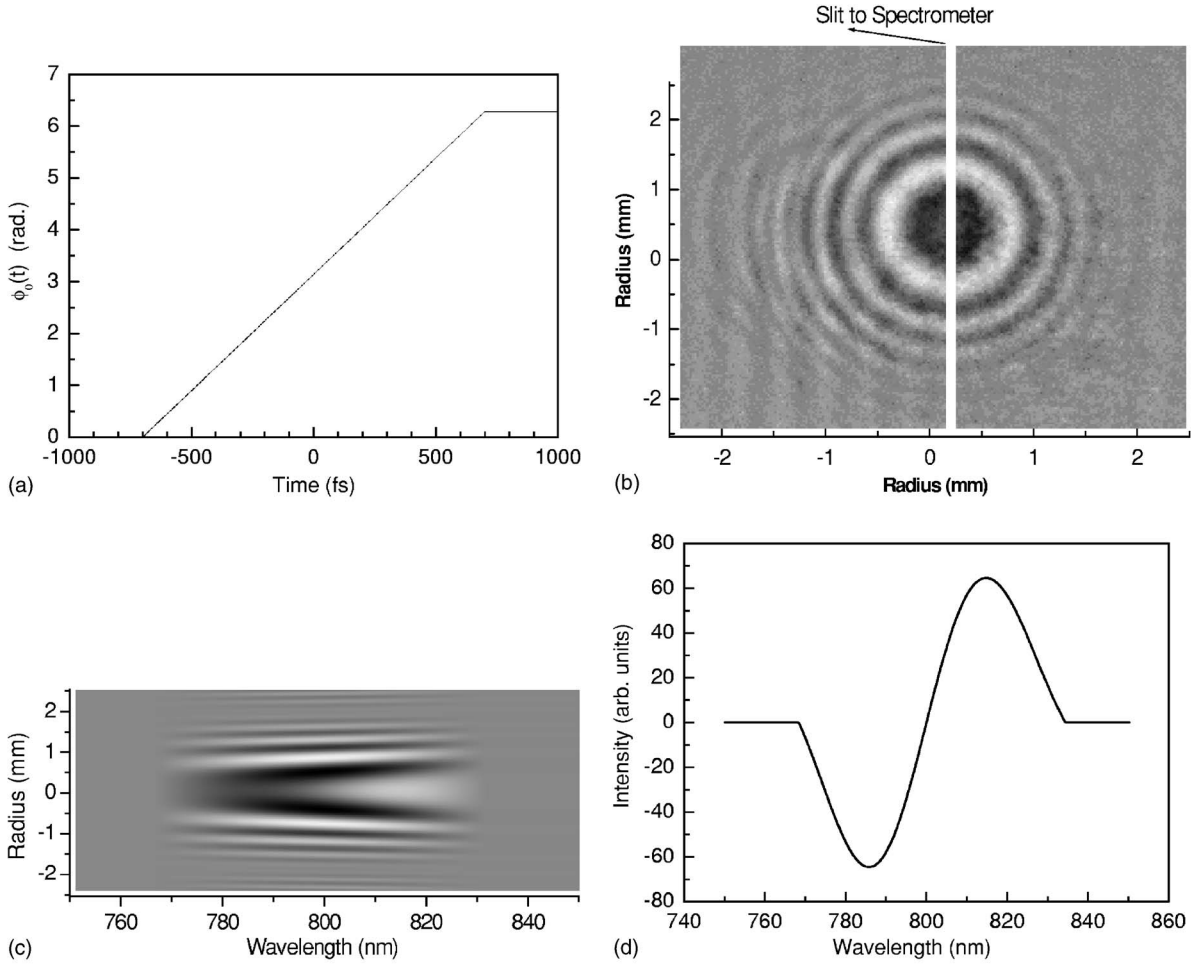

FIG. 7. (a) Linearly varied phase shift with time. (b) Measured 2D diffraction fringe by a CCD camera. (c) The recorded diffraction fringes in frequency and space domain where a linearly negative chirped laser beam is employed. (d) The light intensity as a function of laser wavelength at the center of the fringes in (c).

experienced by the probe beam. The length and the radius of the plasma channel are set at 1.8 cm and 25 μm, respectively, which are close to the measurement. If the radial refraction is not considered, the phase shift experienced by the probe beam can be calculated by a direct integration $\phi(r) = (2\pi/\lambda)[n_e(r)/2n_c]l_{channel}$, which has the same Gaussian profile as the electron density. The dashed lines in Fig. 6 show the directly integrated phase shift when the electron densities are set at $5\times10^{15}, 2\times10^{16}$, and 5×10^{16}cm^{-3}, respectively. However, the phase shift $\phi(r)=\int_0^{l_{channel}}(2\pi/\lambda)\times[n_e(r)/2n_c]ds$ at the exit of the plasma channel calculated by solving the above equation of ray tracing [9] at the corresponding electron densities is shown in the solid line respectively in Fig. 6. It can be seen that in our case when the electron density is lower than 10^{17} cm^{-3}, the phase shift $\phi(r)$ experienced by the probe beam due to the radial refraction has a small difference from the direct integrated phase shift although the diameter of the phase shift $\phi(r)$ increases a little due to refraction of the plasma channel when the electron density is 5×10^{16} cm^{-3}. By comparison, in Ref. [6] where a long filament of 1.5 m would deviate the probe beam from its path more seriously, the measured electron density there has been revised to be around 10^{16}–10^{17} cm^{-3} which is in agreement with our measurement of electron density in the filament. For the method proposed here in this paper, the electron density and channel size can be both measured with a higher precision and sensitivity when the electron density is not too high ($<10^{17}$ cm^{-3} in our case) or the length of the measured plasma channel is not too long. However, using a probe beam with a shorter wavelength such as frequency doubled of 800 nm can decrease the effect of radial refraction. Moreover, the measured length of the plasma channel can be shortened to decrease the effect of radial refraction by changing the delay between the pump and the probe laser pulses in our case if the electron density is much higher.

IV. PROPOSAL OF TIME-RESOLVED MEASUREMENT BY USING LINEARLY CHIRPED LASER PULSE

Time-frequency domain techniques such as frequency resolved optical gating (FROG), multipulse interferometric FROG (MI-FROG), and spectral interferometry (SI) have been widely employed in many experiments to measure ultrafast ionization dynamics of laser-irradiated gases [18–20], laser-cluster interactions [21,22], and laser-driven wakefields

[23]. Here in this section a different time-frequency technique called linearly chirped longitudinal diffractometry is to be proposed as follows based upon the above results.

The experimental setup for this method is similar to that shown in Fig. 1, except that the probe beam would be a linearly chirped laser pulse which co-propagates with the plasma filament in the same direction, and the CCD camera would be replaced by a two-dimensional (2D) spectrometer with a CCD camera. The light field of the linearly chirped laser beam which is assumed to be a Gaussian function in temporal-spatial domain has the following form:

$$U_0(r,t) = \exp(-ar^2)\exp[-j\phi(r,t)] \times \exp[-Tt^2 + j(\omega_0 t + bt^2)], \tag{10}$$

where $2b$ is the chirp rate, ω_0 is the central frequency of the probe beam, and the phase shift $\phi(r,t)$ caused by the plasma is assumed to be

$$\phi(r,t) = \begin{cases} \phi_0(t) & r \leqslant r_c(t) \\ 0 & r > r_c(t). \end{cases} \tag{11}$$

$r_c(t)$ is the radius of the plasma filament, the accumulated phase $\phi(r,t)$ is related to the plasma density $n_e(t)$ by the relation $\phi_0(t) = (2\pi/\lambda)[n_e(t)/2n_c]l_{channel}$, where n_c is the plasma critical density and $l_{channel}$ is the length of the plasma filament. As discussed in Sec. III, the diffracted light field in the recording screen can be expressed as

$$\begin{aligned} U_{yes}(r,t) &= \exp(jA_0 r^2)\left[\int\int_0^{r_c} + \int\int_{r_c}^{\infty} U_0(\xi,\eta,t)\exp[jA_1(\xi^2+\eta^2)] \times \exp[-jA_2(x\xi + y\eta)]d\xi d\eta \right] \\ &= [E_0(r)e^{-j\phi_0(t)} + E_1(r)]f(t), \end{aligned} \tag{12}$$

where $f(t) = \exp[-Tt^2 + j(\omega_0 t + bt^2)]$. The spectrum of the diffracted light field in the frequency domain is the Fourier transform of the above equation in time domain and is written

$$\begin{aligned} U_{yes}(r,\omega) &= \text{F.T.}\{[E_0(r)e^{-j\phi_0(t)} + E_1(r)]f(t)\} \\ &= [E_0(r)e^{-j\varphi_0(\omega)} + E_1(r)]F(\omega). \end{aligned} \tag{13}$$

$F(\omega)$ is the Fourier transformation of $f(t)$, $\varphi_0(\omega) \approx \phi_0(t(\omega)) + \frac{1}{2}A(\partial\phi_0/\partial t)^2/[1-2A(\partial^2\phi_0/\partial t^2)]$, and $A = \frac{1}{2}[b/(T^2+b^2)]$ [22]. If the blueshift satisfies $\frac{1}{2}A(\partial\phi_0/\partial t)^2 \ll \phi_0(t(\omega))$, a simple linear mapping approach to extract phase shift as $\phi_0(t(\omega)) = \varphi_0[A(\omega-\omega_0)]$ gives a good result with less distortion [18,22]. Therefore the recorded diffraction pattern in the frequency domain in the direction of the slit of the spectrometer can be written as

$$I_d(y,\omega) = I_{yes}(y,\omega) - I_{no}(y,\omega) = E_0(y,\omega)e^{-j\varphi_0(\omega)}E_1^*(y,\omega) - E_0(y,\omega)E_1^*(y,\omega) + \text{c.c.} = -\operatorname{sgn}(A_1)C\pi r_c^2 \frac{1}{\sqrt{a^2+A_1^2}} \times \exp(-b_0 y^2)\frac{J_1(A_2 r_c y)}{A_2 r_c y}\cos[b_1 y^2 - \varphi_0(\omega)/2]\sin[\varphi_0(\omega)/2]F^2(\omega). \tag{14}$$

For a linearly varied phase shift $\phi_0(t)$ with time as shown in Fig. 7(a), the 2D spatial diffraction fringes would be shown in Fig. 7(b). However, if we use a linearly negative chirped laser pulse (1.5 ps) with a bandwidth of 45 nm (full width at half maximum) and a spectrometer of which the slit is placed in the radial direction of the fringes in Fig. 7(b), the recorded diffraction fringes $I_d(y,\omega)$ in frequency and space domain would be like that shown in Fig. 7(c). At different wavelength λ, the fringe pattern $I_d(y,\omega)$ shown in Fig. 7(c) is proportional to $\cos[b_1 y^2 - \varphi_0(\omega)/2]\sin[\varphi_0(\omega)/2]F^2(\omega)$, which is determined by the phase shift $\varphi_0(\omega)$. For a linearly negative chirped laser pulse, the blue light (short wavelength) walks in front of the red light (long wavelength), therefore the phase shift $\varphi_0(\omega)$ increases as the wavelength increases for the phase shift $\phi_0(t)$ shown in Fig. 7(a). From Fig. 7(c), the phase shift $\varphi_0(\omega)$ at different wavelength λ can be calculated by fitting the fringe pattern $I_d(y,\omega)$ with Eqs. (14) as discussed in Sec. III, and thus the phase shift $\phi_0(t)$ in the time domain can also be obtained by using a simple linear mapping approach $\phi_0(t(\omega)) = \varphi_0[A(\omega-\omega_0)]$ or a full Fourier extraction $e^{-j\phi_0(t)}f(t) = \text{F.T}^{-1}[e^{-j\varphi_0(\omega)}F(\omega)]$ [18,20–22]. The reconstruction of the phase shift $\phi_0(t)$ from $\varphi_0(\omega)$ will be that shown in Fig. 7(a). The time resolution is $\Delta t = 2\pi/\Delta\omega$ for a full Fourier extraction, and $\Delta\omega$ is the full spectral width of the probe laser. The light intensity as a function of laser wavelength at the center of the fringes in Fig. 7(c) is also shown in Fig. 7(d), which corresponds to $I_d(0,\omega)$ and is proportional to $\sin(\varphi_0(\omega))F^2(\omega)$. It reflects the change of phase shift over a period from 0 to 2π in a single measurement. This method proposed here could be used to time-resolved investigate ultrafast ionization dynamics of laser-irradiated gas, laser interaction with cluster beam, etc. It can be achieved by a single shot, and shot to shot fluctuations can be avoided. Since the diffractometry proposed here is sensitive to the phase shift, it can be used for the measurement of much smaller phase shift compared to the Michelson or Wollaston interferometry [6,10]. The effect of refraction can be avoided if the phase shift is small.

V. SUMMARY

In order to have an insight into the temporal evolution of the electron density in the weak plasma channel where the electron density is expected to be very low, a pump-probe back longitudinal diffractometry has been developed to measure the electron density of less than 10^{16} cm^{-3}, which is sensitive to the phase and channel size. An analytical reconstruction method of phase shift and channel size has been given. The measurable sensitivity of phase shift is able to be less than one-twentieth wavelength, which is higher than that of Michelson interferometric methods, and the measurable electron density can be extended to less than 10^{15} cm^{-3}. Moreover, a time-frequency technique called linearly chirped longitudinal diffractometry is proposed to time-resolved investigate ultrafast ionization dynamics of laser-irradiated gas, laser interaction with cluster beam, etc.

ACKNOWLEDGMENTS

This work was supported by the major basic research project of Chinese Academy of Sciences, the Chinese High-Tech Program, the Chinese National Major Basic Research Development Program, the National Natural Science Foundation of China (Contract Nos. 19774058 and 69925513), and the Shanghai Center for Applied Physics (Contract No. 99JC14006).

[1] J. Kasparian, M. Rodriguez, G. Méjean, J. Yu, E. Salmon, H. Wille, R. Bourayou, S. Frey, Y.-B. André, A. Mysyrowicz, R. Sauerbrey, J. P. Wolf, and L. Wöste, Science **301**, 61 (2003).

[2] H. Pépin, D. Comtois, F. Vidal, C. Y. Chien, A. Desparois, T. W. Johnston, J. C. Kieffer, B. La Fontaine, F. Martin, F. A. M. Rizk, C. Potvin, P. Couture, H. P. Mercure, A. Bondiou-Clergerie, P. Lalande, and I. Gallimberti, Phys. Plasmas **8**, 2532 (2001).

[3] M. Rodriguez, R. Sauerbrey, H. Wille, L. Wöste, T. Fujii, Y.-B. André, A. Mysyrowicz, L. Klingbeil, K. Rethmeier, W. Kalkner, J. Kasparian, E. Salmon, J. Yu, and J.-P. Wolf, Opt. Lett. **27**, 772 (2002).

[4] O. G. Kosareva, V. P. Kandiddov, A. Brodeur, C. Y. Chien, and S. L. Chin, Opt. Lett. **22**, 1332 (1997).

[5] A. Braun, G. Kom, X. Liu, D. Du, J. Squier, and G. Mourou, Opt. Lett. **20**, 73 (1995).

[6] B. La Fontaine *et al.*, Phys. Plasmas **6**, 1615 (1999).

[7] S. Tzortzakis *et al.*, Phys. Rev. E **60**, R3505 (1999).

[8] A. Talebpour, M. Abdel-Fattah, and S. L. Chin, Opt. Commun. **183**, 479 (2000).

[9] A. Talebpour, M. Abdel-Fattah, A. D. Bandrauk, and S. L. Chin, Laser Phys. **11**, 68 (2001).

[10] Hui Yang *et al.*, Phys. Rev. E **66**, 016406 (2002).

[11] J. Kasparian, R. Sauerbrey, and S. L. Chin, Appl. Phys. B: Lasers Opt. **71**, 877 (2000).

[12] A. Becker, N. Akozbek, K. Vijayalakshmi, E. Oral, C. M. Bowden, and S. L. Chin, Appl. Phys. B: Lasers Opt. **73**, 287 (2001).

[13] W. Liu, S. Petit, A. Becker, N. Akozbek, C. M. Bowden, and S. L. Chin, Opt. Commun. **202**, 189 (2002).

[14] S. Tzortzakis, B. Prade, M. Franco, and A. Mysyrowicz, Opt. Commun. **181**, 123 (2000).

[15] Joseph W. Goodman, *Introduction to Fourier Optics* (McGraw-Hill, New York, 1996).

[16] A. Ting, I. Alexeev, D. Gordon, R. Fischer, D. Kaganovich, T. Jones, E. Briscoe, J. Peñano, R. Hubbard, and P. Sprangle, Phys. Plasmas **12**, 056705 (2005).

[17] A. Yariv, *Quantum Electronics* (Wiley, New York, 1975).

[18] C. Y. Chien, B. La Fontaine, A. Desparois, Z. Jiang, T. W. Johnston, J. C. Kieffer, H. Pepin, F. Vidal, and H. P. Mercure, Opt. Lett. **25**, 578 (2000).

[19] C. W. Siders, S. P. Le Blanc, D. Fisher, T. Tajima, M. C. Downer, A. Babine, A. Stepanov, and A. Sergeev, Phys. Rev. Lett. **76**, 3570 (1996).

[20] K. Y. Kim, I. Alexeev, and H. M. Milchberg, Opt. Express **10**, 1563 (2002).

[21] K. Y. Kim, I. Alexeev, E. Parra, and H. M. Milchberg, Phys. Rev. Lett. **90**, 023401 (2002).

[22] Liu Jiansheng *et al.*, Chin. Phys. Lett. **20**, 1492 (2003).

[23] C. W. Siders, G. Rodriguez, J. L. W. Siders, F. G. Omenetto, and A. J. Taylor, Phys. Rev. Lett. **87**, 263002 (2001).